Swarm based airborne wind measurement

S. Kean*, M. Marino, S. Watkins, A. Mohamed
RMIT University, Melbourne, Australia

ABSTRACT

This paper presents the design and development of a swarm of four wind sensing MAVs equipped with custom four-hole pressure probes to record airspeed and direction at up to 1000Hz. A comparison between a TFI Cobra Probe and the drone system is made during a hovering experiment. Following this an atmospheric boundary layer is measured using the four drones simultaneously. Finally, a preliminary attempt at mapping the wind flow around a shipping container is made.

1 INTRODUCTION

There is a growing desire for a deeper understanding of the local flow conditions within the lower regions of the atmospheric boundary layer. This stems from a number of applications including localized weather predictions, particulate dispersion, wind energy extraction, pedestrian comfort and advanced air mobility (AAM) concepts such as air taxis and micro air vehicles (MAV) for package delivery. Many of these emerging applications will take place in urban environments, which are dominated by mechanical mixing due to high surface roughness and the presence of buildings. This mechanical mixing produces high levels of turbulence that occur at a wide range of spatial and temporal scales, producing a complex spectrum of eddies[1]. Reproducing the full spectrum in a wind tunnel or CFD model is challenging, time consuming and requires accurate modeling of the location and upwind fetch. An alternative is to directly measure the flow field via full-scale experiments. This is typically done using combinations of statically mounted anemometers and long-range sampling devices like SODARs and LIDARs. These techniques are often limited by the placement of devices and the cost of installing masts and other structures to reach a desired location and are inherently expensive and prohibitive. Long range measurements devices are also often unsuitable for studying small scale turbulence as they average over a measurement volume[2]. For these reasons, it is expected that MAV-based measurements could provide a cheap, flexible and configurable solution to collecting short time scale wind measurements in previously inaccessible locations.

A wealth of knowledge already exists regarding the wind loading of structures, however much of this previous work examines wind flows at much longer spatial and temporal scales than are expected to be relevant for these emerging applications. Wind engineering standards vary from country to country, but generally use time averages of 10 minutes in meteorology [3] up to 30 minutes or more as required by the applications for assessing structural loads[4]. For the case of predicting wind energy availability and the placement of micro turbines, Stathopoulos et al. highlight direct measurements as the most dependable method, despite the inherent costs required[5]. However, this is usually not possible during the design phase, as no building exists at the site to mount anemometers on. Hence the use of CFD and wind tunnel modeling as a means to predict the flow environment after construction[6]. Both of these solutions, however, require reliable knowledge of the local inflow conditions at the site to achieve realistic replication. Inflow conditions are usually estimated from standards based from the terrain classification at the measurement location and its fetch[6, 1]. MAVs have been shown to be an effective tool for measuring these inflow conditions by collecting ABL profiles at a variety of terrain conditions[7, 8, 9] including sub-urban and urban environments[10]. In most of the studies these profiles were validated against measurements taken on a static mast.

MAVs have seen increasing use for the measurement of atmospheric phenomena, utilizing both fixed wing and multirotor configurations depending on the studies performed[11]. The flexibility of an airborne platform provides unique benefits, particularly for difficult to reach locations such as around buildings and wind turbines. In the last 5 years there has been a large focus on the use of indirect measurement techniques, where the wind vector is inferred from a kinematic model of the vehicle[12, 13, 14, 15]. This is a cost-effective solution as nearly any off-the-shelf drone can be utilized, provided the kinematics of the vehicle can be accurately modeled. Indirect techniques, however, are generally not suitable for the study of turbulent properties as they spatially average the volume that the drone occupies and rely on the response of the drones control system which varies greatly from platform to platform. Alternatively, direct techniques have also been explored[10, 16, 17], utilizing anemometers mounted on the multirotor to directly sample the flow field. Depending on the anemometer chosen, this can enable the measurement of turbulent properties. A key concern often raised about such systems is ensuring the aircraft does not interfere with the measurements. This is done either by careful placement of the device, post processing corrections to remove influences or a combination of both. Barbieri et. al performed an intercomparison of a collection of meteorology MAVs in a series of field trials and compared the results against a static

*Email address: s3605238@student.rmit.edu.au

mast. In the case of flow sensing, they found that all the multirotors showed good agreement with the tower based measurements, often outperforming their fixed wing counterparts due to the ability to fly stationary relative to the reference instrument[11].

MAVs can also be coordinated in a swarm to collect simultaneous data, allowing for more complex analysis to be performed. Pu et al.[18] Utilized simultaneous measurements with two MAVs using sonic anemometers to develop a gradient map of wind speeds and turbulent intensities in an urban environment. The first MAV was used to measure the upstream flow during the experiment at a fixed reference height, whist the second recorded the flow between buildings. Larger swarms have also been demonstrated such as Wetz et al.[9] comparing indirect wind measurements from 10 MAVs against mast mounted sonic anemometers and lidars, showing that flow structures in time and space could be resolved and compared to static references.

2 OBJECTIVES

To provide a brief overview of the measurement, flight and post processing system, then demonstrate the capability of a swarm of four flying anemometers to provide high frequency wind data. Three experiments will be conducted. A hovering comparison against a TFI Cobra Probe, recording of an atmospheric boundary layer profile and 3D visualization of the wind flow around a shipping container.

3 SYSTEM

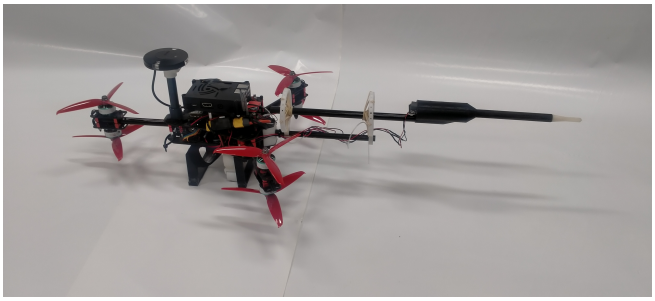

Figure 1: One of four MAVs with measurement system.

The MAVs were designed to provide a stable measurement platform in turbulent and gusty conditions, as well as keep the probe as far away from the rotors as possible. For this reason, a Y6 frame was chosen, as the asymmetry lends itself to mounting the pressure probe on a damped mast (see Figure 1). It is also convenient to use smaller props as it means the probe tip can be closer to the CG of the drone. Prudden et al. previously investigated the interaction between air speed and direction for a similar MAV configuration and determined that at a distance of at least 2.5 rotor diameters air speed was not measurably effected and flow deflection was minimized[19]. As such the probe tip is mounted 3 rotor diameters upstream in the above design. Wind tunnel experiments are planned to validate and potentially correct any angle changes induced by the props.

The measurement system is a custom 4-hole pressure probe designed to be mounted on an MAV. The probe can measure airspeed and direction at 1000Hz and was designed after the TFI Cobra Probe. The probe tip was 3D printed in resin with a tip diameter of approximately 1cm. A batch of the printed probe heads was calibrated and intercompared in a wind tunnel and were found to have no measurable variation between the prints. This means that if the probe head is damaged it can be replaced without needing to re-calibrate in the wind tunnel.

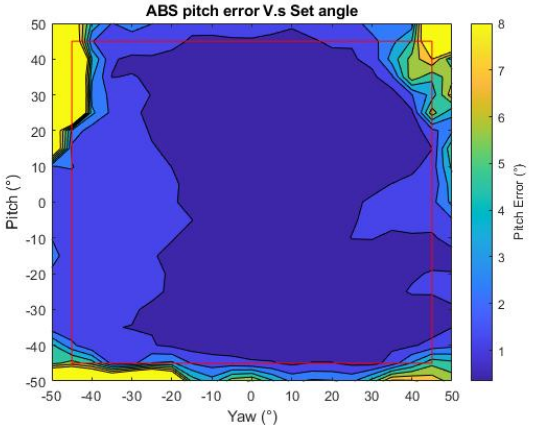

Figure 2: ABS Pitch error

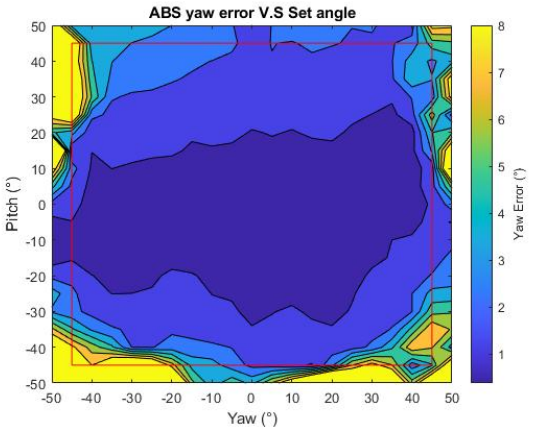

Figure 3: ABS Yaw error

The results of the calibration process showed that the maximum error for pitch, yaw and speed was ±2°, ±2° and ± 5%. The plots in Figure 2 depict this, where the x and y axis correspond to the set pitch and yaw angle of the probe, and the color represents the difference between the measured pitch (Figure 2), yaw (Figure 3) and speed (Figure 4). Six-

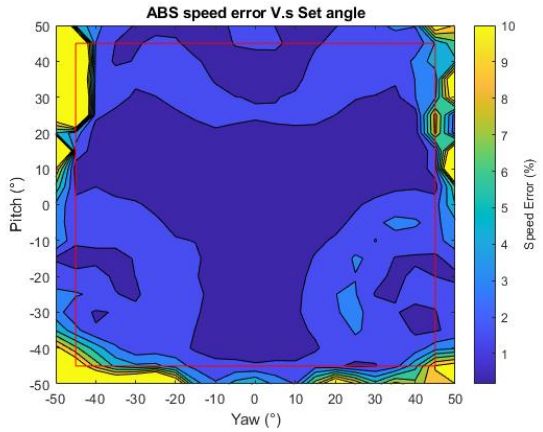

Figure 4: ABS Speed error

teen calibration functions were generated for this data set, using four probe heads and four speeds, nominally 5, 10 and 15 m/s. These can be compared as the calibration surfaces are non-dimensional and Reynolds number invariant[20]. It is worth noting that these values represent the largest errors observed at the extremities of the 45° cone of acceptance which is overlayed in Figure 2 using the red box. Within the first 25 degrees of the origin in both pitch and yaw axis, the error is less than ±1°.

To correctly represent the wind vector in an Earth-centric coordinate system, the motion and attitude of the drone needs to be corrected for. This is done using the flight log from the drone, and using a sequence of transformations based on the equations in Prudden et al[16]. These equations are used to subtract any airspeed induced by the motion of the drone both linear and rotational. This means that the drones can be in motion when recording wind data, although the most accurate results are achieved when close to constant motion is maintained. Once this is complete, the data is low passed and down sampled to 120Hz. This is conveniently below the blade pass frequency, one of the largest sources of mechanical noise.

Another challenge for this is system is ensuring temporal coherence between each of the separate MAVs. The GPS UTC time provided in the flight log is not very reliable, showing significant drift between separate drones. By interfacing a raspberry Pi with the flight controller, the electrical trigger of the probe can be recorded with much higher accuracy. The probe is then interfaced with the Pi over USB to record the pressure measurements. The Pi listens to the telemetry port on the flight controller and when a UTC boot time is recorded from the GPS it is compared with Pi's own UTC time. The difference is used to align the two flight logs under the assumption that the electrical signal is perceived simultaneously by the Raspberry Pi and the probe. This also enables the Pi to publish probe sensor data into the MAVLINK telemetry stream. This data is transmitted via the telemetry radio to the ground control station for use during experiments. A screenshot of the swarm control interface is shown in Figure 5.

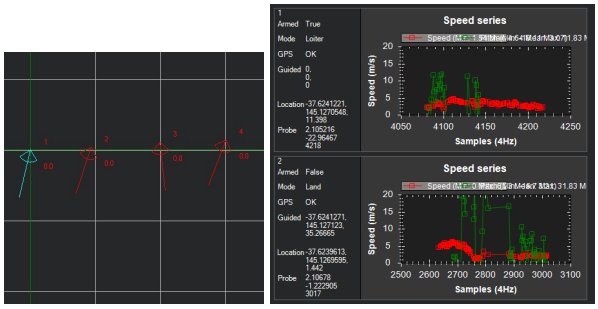

(a) (b)

Figure 5: (a) GCS Drone formation view (b) GCS drone status and probe view

The swarm control system is a modified version of the beta swarm feature included in Mission Planner- the open source ground control station(GCS). The modifications include a critical bug fix that caused violent oscillations in the vehicles yaw axis, as well as a rewrite of the interface to enable it to be more easily utilized for atmospheric measurement purposes. Conceptually, the swarm system is a formation flight, where each follower vehicle receives guided mode commands from the GCS. The interface enables the vertical and horizontal offsets of each vehicle to be specified relative to the flight leader. It is then up to the autopilot of each vehicle to achieve these waypoints and maintain the correct locations. Although this is not an intelligent or adaptive control system, its more than sufficient to support the atmospheric measurements that this research requires. Having a centralized control system also enables the mission to be easily modified during a flight, something that is challenging with preprogrammed waypoint controls. The final advantage of this system, is that the swarm control system is only concerned with high level vehicle commands, leaving flight operations to the onboard flight controller, meaning that the control system is agnostic of the vehicle hardware.

4 EXPERIMENTS

4.1 Hovering comparison

To validate the whole system in combination, a flight experiment was performed where an MAV was hovered next to a cobra probe on a 3m mast for approximately two minutes. The drone was positioned with its tip 1m to the right of the cobra probe and facing in approximately the same direction. Both the cobra probe and the drone were recording at 1000Hz. Figure 6 shows good agreement for the low frequency components and the average speed over the entire sample was 4.95m/s for the cobra probe and 5.13m/s for the MAV. Turbulent intensity is a non-dimensional measure of

the fluctuating component of a velocity time series. It can be calculated along each component axis as shown in (1), or as a total as shown in(2).

$$Ti_u = \frac{\sigma_u}{\overline{V}}, Ti_v = \frac{\sigma_v}{\overline{V}}, Ti_w = \frac{\sigma_w}{\overline{V}} \quad (1)$$

$$Ti_{total} = \frac{\sqrt{\sigma_u^2 + \sigma_v^2 + \sigma_w^2}}{\overline{V}} \quad (2)$$

The turbulence intensities, shown in Table 1, also showing good agreement. Some differences are to be expected between the two measurements, especially in the short time scale. Such velocity fluctuations can occur across very small spans and have been previously measured in [21].

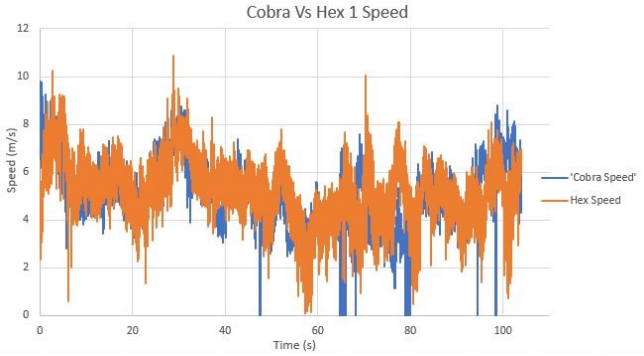

Figure 6: Wind speed comparison between static cobra probe and flying MAV probe

	Avg. Speed(m/s)	Total	Ti_u	Ti_v	Ti_w
MAV	5.13	0.24	0.24	0.29	0.2
Cobra	4.95	0.22	0.26	0.24	0.13

Table 1: Comparison between Average speeds and turbulence intensities.

4.2 *Atmospheric boundary layer profile*

Atmospheric boundary layer profiles provide information about how the wind interacts with the local environment. As the wind flows across the surface of the planet, it interacts with any buildings or objects in its path. This creates a decaying spectrum of turbulence close to the ground. As a result, wind speed generally increases while turbulence intensity decreases with altitude exponentially. The power law is one model of wind profile used within the lower ABL and is shown in (3).

$$u(z) = u(z_0) * (\frac{z}{z_0})^a \quad (3)$$

Assuming neutral stability conditions, the exponent a is entirely dependent on the roughness of the local terrain, and therefore can be calculated by directly measuring the wind at multiple heights. Standards provide typical ranges for the curve exponent based on the roughness classifications of different terrains. Forests and sub-urban areas, for example, are listed by Emeis et al. as being 0.28-0.4 [22]. The experiment was performed at Greensborough Model Aircraft Club, in a flat open field. Roughly 100m upwind of the measurement site is a row of trees, approximately 20m in height, followed by 2km of sparsely wooded parkland. The landscape quickly develops into an urban sprawl that continues towards Melbourne. To measure the wind speeds, the drones were coordinated as a vertical stack at 10m, 30m, 60m and 100m above ground level. The wind speed at each height was averaged and the results are shown in Figure 7 (a). The blue curve represents the 4 simultaneously measured points, and the dotted blue line is a best fit to the power law. The orange curve is a theoretical power law with an exponent value of 0.35 for comparison. This value was chosen as the 'average' for this terrain category.

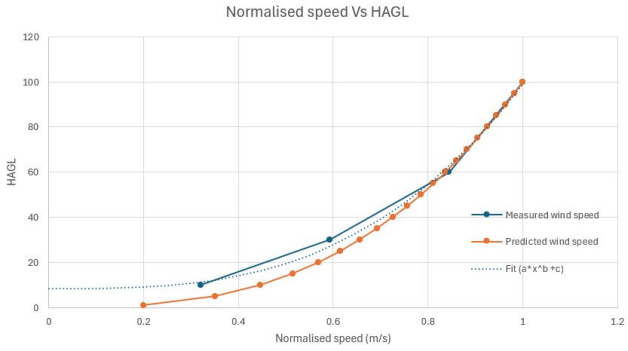

(a)

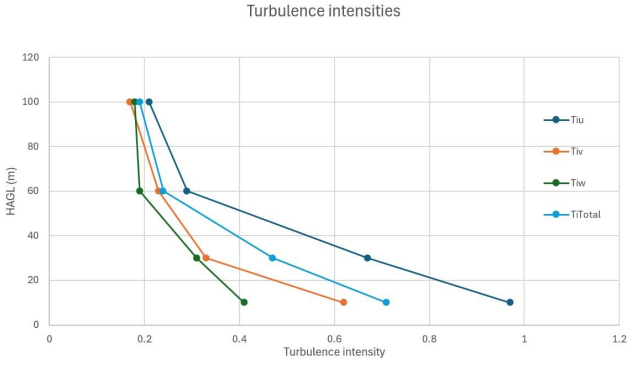

(b)

Figure 7: (a) Wind speed v.s HAGL. (b) Turbulent intensity v.s HAGL

Fitting a curve to the measured data, an exponent of 0.33 is calculated. This value is a surprisingly good match to the theoretical model given the simplifications made. The fitted curve also shows that the y-intercept(displacement height), the height at which zero wind speed could be expected, to be

at around 8m. This is reasonable given that the upwind trees effectively created a wind shadow at the measurement site. It's worth noting that no displacement height was used for the theoretical power curve, as the equations generally don't include it and so typical values are not available. This is not the case for the logarithmic wind model in which a displacement height is specified, and typical values can be found in the ESDU data sheets[4]. Although inter comparing wind models is a challenging task unto itself, the typical displacement heights can be compared as they simply represent a translation along the y axis. The displacement values provided for urban and fairly level wooded country is between 5 and 10m, which is a good match to the measured data. Figure 7 (b) shows the change in turbulent intensities against altitude. Close to the ground a significant decrease in the w component of turbulence intensity is seen when compared to the other components. This aligns with the theory and is caused by the interaction of eddies with ground. As the eddies cannot pass through the ground, they effectively 'smear' their energy into the other two component directions. Its expected the combination of fetch terrain changes and the close upwind trees increased the levels of turbulence close to the ground when compared to the typical theoretical model. The indication of an 8m displacement height from the measured drone data also helps to explain the high turbulence levels recorded by the drones at lower altitudes.

4.3 Container flow mapping

As it is ultimately intended for the drones to be used to study air flows around buildings and in urban areas, it is important to ensure that they can safely fly and record data in regions of interest. An example of this would be the shear layer that occurs near the roof of a cuboid building. A shear layer is characterized by the rapid velocity changes that occur as a result of the airflow compressing and accelerating around the object. Measuring this has particular relevance to AAM applications as any aircraft landing/taking off on a roof or vertiport has to transition through this region safely.

A single drone was manually flown around the area where the shear layer was expected to form for approximately 3 minutes and its flight path is shown by the blue line in Figure 9(a). During this time the drone faced into wind which blew from the south. The samples recorded were then processed into a 3D volume of point measurements. This was done by creating a voxel grid at the location of the flight path. The voxel grid is represented top down by the pink box in Figure 9 (a). The size of the grid cell is then used to spatially average the measurements which can then be represented using 2D slices, cones and streamlines as shown in Figure 6 and Figure 7. The grid size for below data is 0.75m.

Figure 9 (a) and Figure 9 (b) show the vertical component of wind at two different spans along the container's length. An updraft was measured along the leading edge and a down draft just behind it. It is assumed this is associated with the

(a) Satellite view of flight path

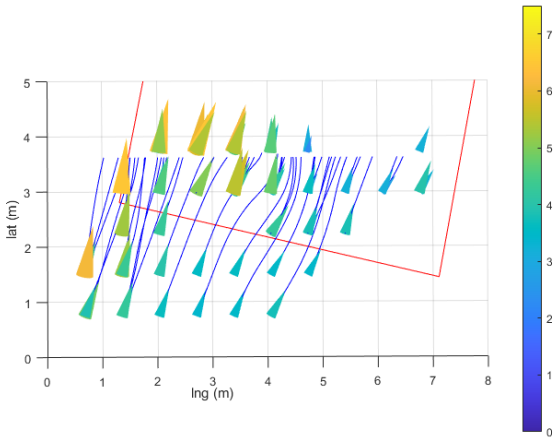

(b) Top down view of velocity magnitude

Figure 8: (a) Satellite view of container. (b) Top down view of velocity magnitude.

shear layer that would develop over a bluff body. Turbulence intensities were also calculated across the volume, and were shown to be higher closer to the surface of the container as shown in Figure 9 (c).

A flight path that more evenly distributes measurement points and using multiple drones would provide a clearer visualization of flow around the container, but this preliminary test shows promise. The use of AI for sparse wind field prediction is currently being researched[23, 24] and data sets such as this may in the future be completed using such predictions.

5 CONCLUSION

A swarm of four flying anemometers has been developed utilizing four-hole pressure probes to record wind speed and direction at high rates. An experiment that compared

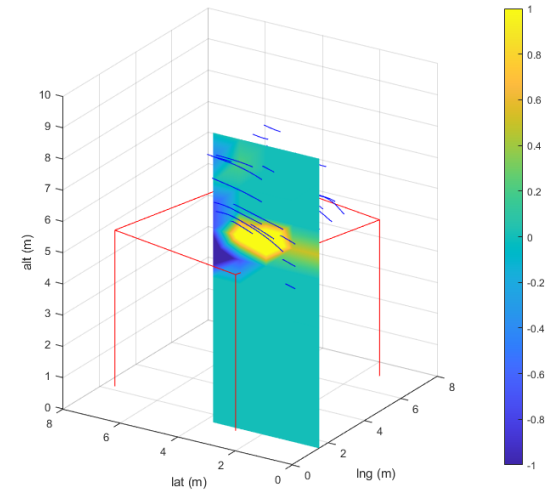

(a) Vertical component of wind at x=1.5m

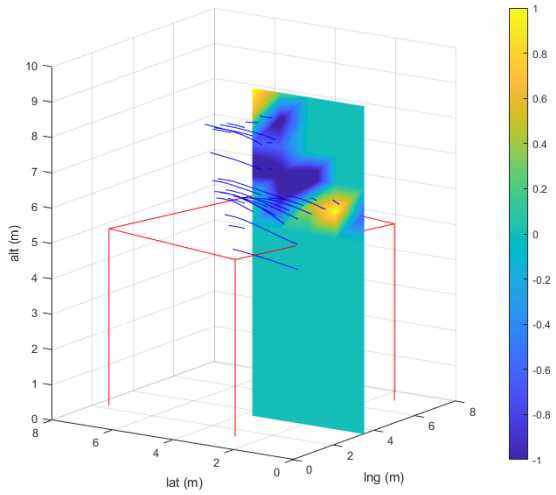

(b) Vertical component of wind at x=3.5m

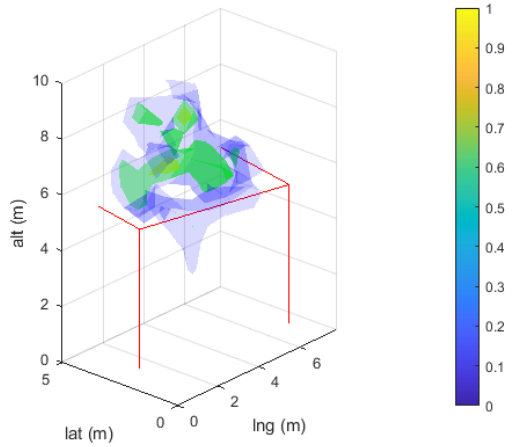

(c) Total turbulence intensity

Figure 9: (a)Vertical component of wind at x=1m. (b)Vertical component of wind at x=3.5m. (c) Total turbulence intensity

wind speed and turbulence intensities against a cobra probe that was mounted on a mast was conducted and showed good agreement. An atmospheric boundary layer profile was recorded using all 4 drones simultaneously and the terrain exponent was calculated showing good agreement with the theoretical model. Finally, a preliminary flow mapping trial was performed around a shipping container in high winds as a scale analogy for building. An updraft was successfully measured along the leading edge of the container. In the future, full scale experiments utilising all 4 drones will be conducted on the rooftop of a multi story building. Utilising multiple drones will enable the simultaneous capture of wind data for the correlation at multiple locations. This could be used to model the role disturbance of an aircraft within this region of the flow.

REFERENCES

[1] J. C. Kaimal and J. J. Finnigan. *Atmospheric boundary layer flows their structure and measurement*. Oxford scholarship online. Oxford University Press, New York, 1st ed. edition, 1994.

[2] R. M. Hardesty. *LIDAR — Doppler*, pages 1194–1202. Academic Press, Oxford, 2003.

[3] Beurea of meteorology. About forcast models, 2024.

[4] ESDU. Characteristics of atmospheric turbulence near the ground part i: definitions and general information, 1974.

[5] Ted Stathopoulos, Hatem Alrawashdeh, Ayman Al-Quraan, Bert Blocken, Aierken Dilimulati, Marius Paraschivoiu, and Pragasen Pilay. Urban wind energy: Some views on potential and challenges. *Journal of Wind Engineering and Industrial Aerodynamics*, 179:146–157, 2018.

[6] Maryam Al Labbad, Alanna Wall, Guy L. Larose, Fidel Khouli, and Hali Barber. Experimental investigations into the effect of urban airflow characteristics on urban air mobility applications. *Journal of wind engineering and industrial aerodynamics*, 229:105126, 2022.

[7] Sara Alaoui-Sosse, Pierre Durand, Patrice Medina, Philippe Pastor, Marie Lothon, and Iuri Cernov. Ovli-ta: An unmanned aerial system for measuring profiles and turbulence in the atmospheric boundary layer. *Sensors (Basel, Switzerland)*, 19(3):581, 2019.

[8] Joachim Reuder, Marius O. Jonassen, and Haraldur Ólafsson. The small unmanned meteorological observer sumo: Recent developments and applications of a micro-uas for atmospheric boundary layer research. *Acta geophysica*, 60(5):1454–1473, 2012.

[9] Tamino Wetz, Norman Wildmann, and Frank Beyrich. Distributed wind measurements with multiple quadrotor unmanned aerial vehicles in the atmospheric boundary layer. *Atmospheric measurement techniques*, 14(5):3795–3814, 2021.

[10] Zhengnong Li, Ou Pu, Yueyue Pan, Bin Huang, Zhefei Zhao, and Honghua Wu. A study on measuring the wind field in the air using a multi-rotor uav mounted with an anemometer. *Boundary-layer meteorology*, 188(1):1–27, 2023.

[11] Lindsay Barbieri, Stephan T. Kral, Sean C. C. Bailey, Amy E. Frazier, Jamey D. Jacob, Joachim Reuder, David Brus, Phillip B. Chilson, Christopher Crick, Carrick Detweiler, Abhiram Doddi, Jack Elston, Hosein Foroutan, Javier González-Rocha, Brian R. Greene, Marcelo I. Guzman, Adam L. Houston, Ashraful Islam, Osku Kemppinen, Dale Lawrence, Elizabeth A. Pillar-Little, Shane D. Ross, Michael P. Sama, David G. Schmale, Travis J. Schuyler, Ajay Shankar, Suzanne W. Smith, Sean Waugh, Cory Dixon, Steve Borenstein, and Gijs de Boer. Intercomparison of small unmanned aircraft system (suas) measurements for atmospheric science during the lapse-rate campaign. *Sensors*, 19(9):2179, 2019.

[12] Pramod Abichandani, Deepan Lobo, Gabriel Ford, Donald Bucci, and Moshe Kam. Wind measurement and simulation techniques in multi-rotor small unmanned aerial vehicles. *IEEE access*, 8:1–1, 2020.

[13] Javier Gonzalez-Rocha, Craig A. Woolsey, Cornel Sultan, Nathan Rose, and Stephan F. J. De Wekker. *Measuring atmospheric winds from quadrotor motion*. 2017.

[14] Kilian Meier, Richard Hann, Jan Skaloud, and Arthur Garreau. Wind estimation with multirotor uavs. *Atmosphere*, 13(4):551, 2022.

[15] Meir Pachter, Nicola Ceccarelli, and Phillip Chandler. *Estimating MAV's Heading and the Wind Speed and Direction Using GPS, Inertial, and Air Speed Measurements*. 2012.

[16] S. Prudden, A. Fisher, M. Marino, A. Mohamed, S. Watkins, and G. Wild. Measuring wind with small unmanned aircraft systems. *Journal of wind engineering and industrial aerodynamics*, 176:197–210, 2018.

[17] N. Vasiljević, M. Harris, A. Tegtmeier Pedersen, G. Rolighed Thorsen, M. Pitter, J. Harris, K. Bajpai, and M. Courtney. Wind sensing with drone-mounted wind lidars: proof of concept. *Atmos. Meas. Tech.*, 13(2):521–536, 2020.

[18] Li Zhengnong Bao Terigen Chen Zheng Yang Liwei Qin Hua Li Zhen Pu Ou, Yuan Boqiu. Research on the characteristics of urban building cluster wind field based on uav wind measurement, 2023.

[19] Samuel Prudden, A Fisher, A Mohamed, and S Watkins. A flying anemometer quadrotor: Part 1. In *Proceedings of the International Micro Air Vehicle Conference (IMAV 2016), Beijing, China*, pages 17–21.

[20] I. C. Shepherd. A four hole pressure probe for fluid flow measurements in three dimensions. *Journal of fluids engineering*, 103(4):590–594, 1981.

[21] M. Thompson, S. Watkins, C. White, and J. Holmes. Span-wise wind fluctuations in open terrain as applicable to small flying craft. *Aeronautical journal*, 115(1173):693–701, 2011.

[22] Stefan Emeis. *Wind energy meteorology : atmopsheric physics for wind power generation*. Green energy technology. Springer-Verlag, Berlin, Heidelberg, 2013.

[23] Longyan Wang, Meng Chen, Zhaohui Luo, Bowen Zhang, Jian Xu, Zilu Wang, and Andy C. C. Tan. Dynamic wake field reconstruction of wind turbine through physics-informed neural network and sparse lidar data. *Energy*, 291:130401, 2024.

[24] Bingchao Zhang, Ryozo Ooka, Hideki Kikumoto, Chaoyi Hu, and KT Tim. Towards real-time prediction of velocity field around a building using generative adversarial networks based on the surface pressure from sparse sensor networks. *Journal of Wind Engineering and Industrial Aerodynamics*, 231:105243, 2022.